minerals

Article

Lipid Biomarker and Stable Isotopic Profiles through Late Carboniferous–Early Triassic of the Deepest Well MS-1 in the Junggar Basin, Northwest China

Shuncun Zhang [1,3], Tao Wang [1,3], Hui Guo [1,3], Shengyin Zhang [1,3] and Bo Chen [2,*]

1 Northwest Institute of Eco-Environment and Resources, Chinese Academy of Sciences, Lanzhou 730000, China
2 Guangxi Key Laboratory of Green Chemical Materials and Safety Technology, Beibu Gulf University, Qinzhou 515000, China
3 Gansu Key Laboratory of Petroleum Resources, Lanzhou 730000, China
* Correspondence: cbo-11@163.com

Abstract: The Carboniferous–Triassic period was an important stage of global sea–land transformation, with coal formation in the Carboniferous, biological extinction at the end of the Permian, and global drought in the Triassic. The MS-1 well in the Mosuowan High of the Junggar Basin is the deepest well drilled in Northwestern China. In this paper, we investigate the sedimentary environment and climate evolution of the Mosuowan area in the central Junggar Basin during the Late Carboniferous–Early Permian by the petrothermal, lipid biomarker, and isotopic composition of mud shale core samples, and explore the tectonic–climatic events and Central Asian orogenic belt evolution driving the sedimentary environment. The study shows that the organic matter from the Upper Carboniferous to the Lower Permian is at a mature stage, but biomarkers maintained the primary information although the organic matter was subjected to thermal evolution. In the late Carboniferous period (Tamugan Formation), the study area was a closed remnant sea with a relatively humid climate, triggering lush terrestrial vegetation and high organic carbon content in the sediments, which had the potential to evolve into natural gas. During the Xiazijie Formation of the Middle Permian, tectonic activity shifted to the subsidence period, and the salinity of the water decreased after a large input of fresh water. The lake basin area expanded, and the content of aquatic organisms continued to increase. As the Lower Permian stratigraphy is missing, this sea–land transition seems to jump. The low and upper Urho Formations of the Middle–Upper Permian are a deltaic foreland deposit, and geochemical indicators show an overall lake retreat process with a continuous increase in organic matter content of terrestrial origin. The lithologic assemblage of the Triassic Baikouquan Formation is braided river deltaic sedimentation with migration of deposition centers of the lake basin. In conclusion, the Late Carboniferous–Early Permian period was influenced by global changes, Paleo-Asian Ocean subduction, and continental splicing, which resulted in a continuous increase in terrestrial organic matter, water desalination, and oxidation-rich sediments in the Mosuowan region, but the P–T biological mass extinction event was not recorded.

Keywords: geochemistry; environment; tectonic evolution; Carboniferous–Triassic; Junggar Basin

Citation: Zhang, S.; Wang, T.; Guo, H.; Zhang, S.; Chen, B. Lipid Biomarker and Stable Isotopic Profiles through Late Carboniferous–Early Triassic of the Deepest Well MS-1 in the Junggar Basin, Northwest China. *Minerals* **2022**, *12*, 1299. https://doi.org/10.3390/min12101299

Academic Editors: Marianna Kulkova and Dmitry Subetto

Received: 14 September 2022
Accepted: 14 October 2022
Published: 15 October 2022

1. Introduction

Between the Carboniferous and Triassic periods, north China experienced global events such as coal-forming movements, paleo-oceanic closures and land emergence, and the Permian–Triassic biological mass extinction [1,2]. The Junggar Basin is located at the southwest edge of the Central Asian orogenic belt, where it is the key part of the intersection of the Siberian plate, the Kazakhstan plate, and the Tarim plate. The Carboniferous of Junggar was characterized by the subduction of the ancient Asian Ocean and regional volcanic activity. The Paleozoic–Mesozoic period experienced collisional basin formation, faulting, subsidence, and regenerated foreland basin stages. Meanwhile, the Paleozoic–Mesozoic was also an important stage for hydrocarbon source rock and reservoir development in the Junggar Basin, and several Permian–Triassic hydrocarbon-bearing sags are located in the central part of the basin, such as Mahu Sag, Jimsar Sag, Shawan Sag, etc. [3–5]. At present, sand and conglomerate, dense sandstone, and oil shale of the Permian–Triassic in the northwest margin of the Junggar Basin have become an important, prospective oil and gas reservoir [6,7].

The sedimentation evolution of the Junggar Basin was not only influenced by global tectonic–climatic events but also deeply constrained by the accretionary and extension of the Central Asian orogenic belt. The evolution of the Junggar Basin from the Paleozoic to the Mesozoic was closely related to the subduction and subsidence of the Paleo-Asian Ocean in the northern Xinjiang region. During the Carboniferous period, the Junggar Basin developed several ophiolite belts and regional volcanic clastic rocks. The central part of the basin mainly experienced mechanical subsidence in the Early Permian, thermal subsidence with post-fracture in the Middle Permian, and tectonic inversion during the Late Permian–Early Triassic [8–10]. Paleozoic calc-alkaline volcanic rocks on the perimeter of the basin are the main source of sediments, and the braided, river-fan, deltaic, shallow lake phase sediments were developed from the mountain front region to the lake. The paleontological data show that the northern part of the Junggar Basin experienced four important paleoclimatic events from the Carboniferous to the Triassic period: the Late Carboniferous cooling event, the Middle Permian greenhouse event, the Late Permian–Early Triassic drought event, and the Middle to Late Triassic humid event [11–14].

A large number of geochemical studies have been carried out on volcanic and sedimentary rocks in the Junggar Basin, mainly focusing on tectonic environment discrimination, hydrocarbon source rock evaluation, and sedimentary environment reconstruction in the Carboniferous and Permian systems [15–17]. Geophysical data and sedimentary rock records from the drilled strata have also been used to map the depositional environment [18–20]. However, there is still a lack of regional, continuous, geochemical data for reconstructing the environmental changes from the Carboniferous to Triassic period. In this study, core samples from the deepest well, MS-1, in the Junggar Basin were analyzed for pyrolysis, lipid biomarkers, and carbon isotopic compositions. We studied the composition of the sedimentary organic matter, depositional environment, and climatic evolution of Mosuowan High in the central Junggar Basin during the Carboniferous–Triassic period. The global, tectonic–climatic events and the evolution of the Central Asian orogenic belt which drove the depositional environment of the Junggar Basin are further discussed.

2. Geological Setting

The Junggar Basin is located between the Altai and Tian Shan mountains in Xinjiang, China (92°00′–95°30′ E, 43°20′–45°00′ N) (Figure 1). It is a Late Carboniferous–Quaternary sedimentary basin with a total area of about 130,000 km^2. The Junggar Basin is one of the largest, superimposed, hydrocarbon-bearing basins in northwest China, and its geotectonic position is located at the intersection of three major plates: the Siberian Plate, the Kazakhstan Plate, and the Tarim Plate [21,22]. The formation and evolution of the Junggar Basin were closely related to the subduction and subsidence of the ancient Asian Ocean in the northern Xinjiang region [23–25]. Numerous ophiolite belts are exposed in the West Junggar region, including many ophiolite belts such as Dalabut, Baijiantan, Barrek, Tangbal, and Mayil, which are key evidence of the extinction of the multi-island arc oceanic crust suture [22,26–28]. Based on the Permian tectonic features and late tectonic transformation in the basin, the Junggar Basin is divided into six primary tectonic units, including the Western Uplift, the Eastern Uplift, the Luliang Uplift, the Tianshan Foreland Depression, the Central Depression, and the Ulungu Depression (Figure 1) [29,30].

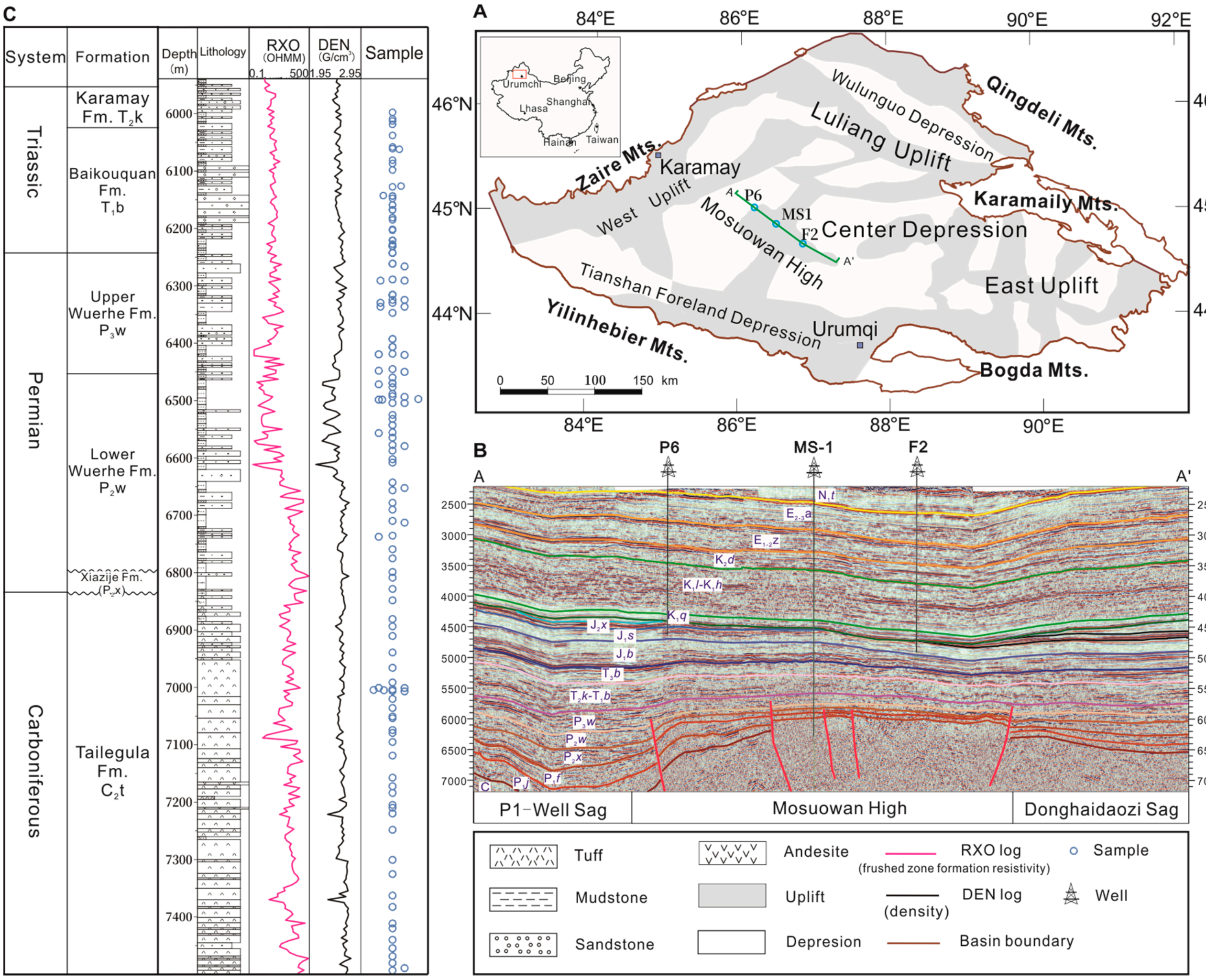

Figure 1. (**A**) Map of sampling location in Junggar Basin, China. (**B**) Seismic profile of well P6, MS-1, F2. (**C**) Detailed stratigraphic column of the sampled interval.

The MS-1 well is located in the Mosuowan Uplift in the Junggar Basin Central Depression, which is a typical basement uplift. The two flanks in the middle of and to the east of the Mosuowan Uplift have developed northwest-trending, geodesic, spreading reverse faults (Figure 1), which have opposite tendencies and make the Mosuowan Uplift have the morphology of a back-breaking block [31]. The stratigraphy drilled in the Carboniferous–Triassic MS-1 well is the Baikouquan Formation (T_1b), Permian Upper Urho Formation (P_3w), Lower Urho Formation (P_2w), Xiazijie Formation (P_2x), and Carboniferous Tamugang (C_2t) [32]. In the Pre-Carboniferous–Carboniferous period, the central and western part of the Junggar Basin showed an island arc uplift area with calc-alkaline volcanic eruptions. At the beginning of the Permian, it was an island arc uplift zone with a northwest–west trend. With the intensification of denudation and sea level change, the island arc uplift was finally covered during the deposition of the Lower Permian Fengcheng Formation (P_1f). At the end of deposition of the P_2x, fold uplift occurred under the influence of north–south extrusion, and the P_2x was locally erased, and the magnitude of the Mosuowan Uplift increased. The P_2w–P_3w were buried again during the depositional period. The Triassic was the period of stable deposition of the Mosuowan High [33–35].

3. Sample and Experiment

3.1. Sample Collection

In this study, 73 samples were collected from the MS-1 well, including 32 samples from the C_2t, 9 samples from the P_2x, 16 samples from the P_2w, 7 samples from the P_3w, and 9 samples from the T_1b. All of the samples were prepared for the determination of total organic carbon and rock pyrolysis parameters. A total of 64 samples were prepared for gas chromatography mass spectrometry (GC-MS) analysis, and 59 samples were selected for chloroform asphalt "A" stable carbon isotope analysis (Tables S1 and S2).

3.2. Experimental Analysis

Extraction and analysis of saturated hydrocarbons: Powder samples were placed in a Soxhlet extractor and extracted with chloroform for 72 h. The extract was concentrated and purified by passing through a silica gel/alumina (1:1) chromatographic column, and the saturated hydrocarbon fractions were collected by washing with 20 mL of n-hexane four times. The saturated hydrocarbon fractions were run in full scan and selected ion monitoring (SIM) mode by a GC-MS Thermal Scientific DSQ II quadrupole mass spectrometer equipped with a 30 m $\times$ 0.25 mm $\times$ 0.25 μm HP-5 MS column with helium as the carrier gas. The oven temperature was initially set to increase from 80 °C to 320 °C at a rate of 10 °C/ min and held at 320 °C for 20 min. The oven was held at 35 °C for 1 min, then the temperature was increased from 35 °C to 120 °C at a rate of 10 °C/min, then from 120 °C to 300 °C at a rate of 3 °C/min, and, finally, held at 300 °C for 30 min. Detection of the biomarkers, hopanes and steranes, was carried out by monitoring the respective, typical ions: m/z 191 for hopanes, m/z 217 for 5α,14α,17α-steranes, and m/z 218 for 5α,14β,17β-steranes.

Total organic carbon (TOC) and rock pyrolysis: The samples (about 100 mg) were crushed, sieved through a 120 mesh sieve, pretreated with 1 mol/L HCL to remove carbonates from the samples, and then heated to 1200 °C in a pyrolysis oven to obtain the TOC. The sample pyrolysis data were collected using a Rock-Eval II instrument according to the theory of Peter et al. [36]. Where S_1 represents the number of liquid hydrocarbons per unit mass of raw oil rock detected at 300 °C, S_2 represents the yield of caseinate cracked per unit mass of raw oil rock detected at 300–600 °C by heating. If the sediment is still in the mature evolution stage in the buried state, the S_2 peak represents the existing potential of the rock to produce oil. $S_1 + S_2$ characterizes the sum of the number of hydrocarbons already produced and potentially able to be produced in the hydrocarbon source rock, which is called hydrocarbon generation potential, i.e., the total number of hydrocarbons that may be produced by the rock, and it gradually decreases with the depletion of the organic matter hydrocarbon generation potential and the hydrocarbon removal process. The parameter T_{max} (°C) is the Rock-Eval pyrolyzer temperature at which the hydrocarbon compounds are observed to reach their maximum degree of pyrolysis, and this parameter can also indicate the maturity of the hydrocarbon compounds.

Chloroform asphalt "A" isotopic analysis: The carbon isotopic composition of chloroform asphalt "A" was determined offline by MAT 253 gas stable isotope mass spectrometer. The results of the carbon isotope analysis are reported as δ sign relative to the Pee Dee Belemnite (PDB) standard, and the analytical precision of the method was better than ±0.2‰ with reproducibility better than 0.2‰.

4. Results and Discussion

4.1. TOC and Rock Pyrolysis Parameters

The TOC of the gray mudstone, tuff, and dark-gray tuff of C_2t was almost less than 0.50% for all, while the TOC of gray-black tuff and coal was relatively high, with ranges of 0.61%–4.64% and 3.26%–5.53%, respectively. The hydrocarbon potential ($S_1 + S_2$) of the samples in C_2t was 0.25–10.18 mg/g, and the maximum pyrolysis temperature (T_{max}) was 441–502 °C. The TOC of P_2x ranged from 0.05% to 1.16%, with $S_1 + S_2$ and T_{max} of 0.14–0.96 mg/g and 425–468 °C, respectively. The TOC of P_2w and P_3w mudstone ranged from 0.44% to 1.21%, and S_1 + S_2 from 0.29 to 3.41 mg/g, while the T_{max} values were 425–471 °C. The T_1b samples were divided into two groups, the brown-gray, mud-bearing siltstone and the gray mudstone. The TOC of the brown-gray siltstone of the T_1b was very low, 0.15%–0.17%, and the TOC of the gray mudstone section was 0.50%–0.77%, with S_1 + S_2 ranging from 1.26 to 2.83 mg/g and T_{max} values of 430–441 °C (Table S1, Figure 2). In general, only samples from the Late Carboniferous had high organic matter content, hydrocarbon generation potential, and thermal evolution degree. If considered on a regional scale, they can be used as a set of effective hydrocarbon source rocks.

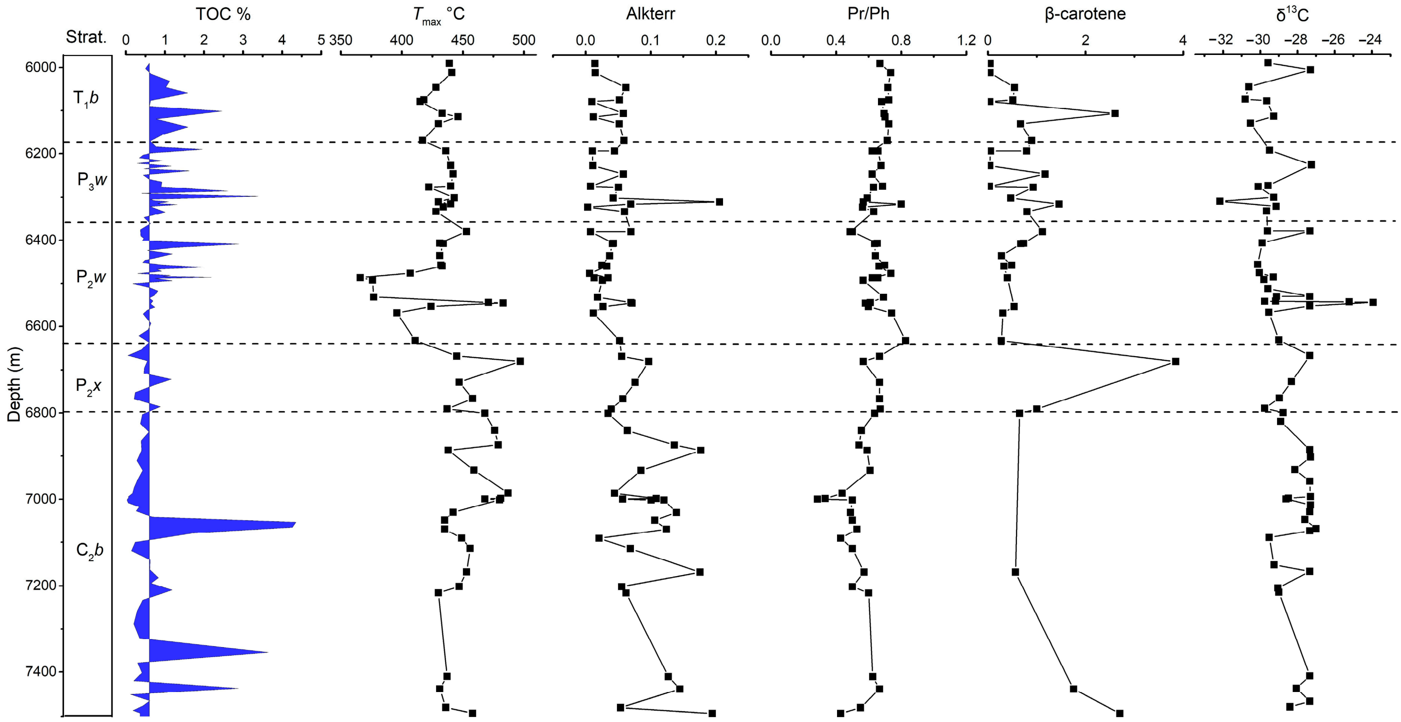

Figure 2. Profiles of rock pyrolysis and organic geochemical parameters in MS-1 well.

4.2. Molecular Geochemistry of Organic Matter

4.2.1. n-Alkanes, Pr/Ph, β-Carotene, and $\delta^{13}C$ of Chloroform Asphalts

The contents and variations of n-alkanes and acyclic isoprene hydrocarbons in the core samples from the C_2t, P_2x, P_2w, P_3w, and T_1b of the MS-1 well were analyzed by gas chromatography. Table 1 summarizes the parameters such as carbon dominance index (CPI_1 and CPI_2) [37], Pr, Ph, β-carotene, and $\delta^{13}C$ of the chloroform asphalt. The n-alkanes of the MS-1 well have single-peak and double-peak distribution patterns, in which the main carbon numbers of the front carbon peak are C_{17} and C_{19}, and the main carbon numbers of the back carbon peak are C_{23} and C_{27}. The n-alkanes of the C_2t are mainly bimodal, with the main carbon peak being C_{19} and C_{23}. The n-alkanes of the P_2x, P_2w, P_3w, and T_1b are mainly single-peaked, with the main carbon peaks of C_{17} and C_{19} (Figure 2). The LMW/HMW of samples in C_2t ranged from 0.4 to 2.36, with a mean value of 1.04. The LMW/HMW of the P_2x, P_2w, and P_3w samples ranged from 1.29 to 1.81, 1.15 to 11.64, and 0.37 to 11.43, respectively, and the LMW/HMW of T_1b ranged from 1.39 to 8.69 with a mean value of 1.04. The CPI_1 and CPI_2 of the C_2t were 0.95–1.31 and 1.04–2.0, respectively, while the CPI_1 and CPI_2 of the P_2x were 1.01–1.1 and 0.82–1.65, respectively, and those of the T_1b were 1.05–1.06 and 1.14–1.19, respectively. The ratio of terrestrial organic hydrocarbons (C_{27}, C_{29}, C_{31}, C_{33}) from higher vascular plant waxes and conifer-derived lipid detritus to the total sum of organic matter is known as the terrestrial index (Alkterr) [38–40], and the Alkterr values of Upper Carboniferous, Permian, and Lower Triassic samples were 0.02–0.19, 0.01–0.21, and 0.01–0.06, respectively.

Table 1. Parameters of δ^{13C} values of n-alkanes, Pr, Ph, β-carotene, and chloroform asphalts from MS-1 well of the Late Carboniferous–Early Triassic.

Strata		β-Carotene /$\Sigma C_{12\text{-}35}$	C_{max} [a]	CPI_1 [b]	CPI_2 [c]	Alkterr [d]	LMW/HMW [e]	Pr/Ph	$\delta^{13}C$ (PDB) [f]
T_1b	Min.	0.04	17	1.05	1.14	0.01	1.39	0.67	−30.81
	Max.	0.9	19	1.06	1.19	0.06	8.69	0.74	−29.28
	Mean	0.53		1.05	1.17	0.05	1.74	0.72	−30.085
P_3w	Min.	0.03	17	1.03	1.11	0	0.37	0.56	−32.17
	Max.	1.46	19	1.06	1.65	0.21	11.43	0.8	−29.15
	Mean	0.79		1.05	1.16	0.04	2.01	0.63	−29.58
P_2w	Min.	0.28	17	1.02	0.98	0.01	1.15	0.49	−30.14
	Max.	1.12	19	1.08	1.25	0.07	11.64	0.83	−23.93
	Mean	0.445		1.07	1.16	0.03	2.29	0.65	−29.3
P_2x	Min.	1	17	1.01	0.82	0.04	1.29	0.57	−29.76
	Max.	3.85	19	1.1	1.21	0.1	1.81	0.67	−28.32
	Mean	2.425		1.05	1.09	0.06	1.57	0.67	−28.705
C_2t	Min.	0.56	17	0.95	1.04	0.02	0.4	0.29	−29.52
	Max.	2.7	27	1.33	2	0.19	2.36	0.67	−27
	Mean	1.2		1.05	1.215	0.105	0.86	0.5	−28.405

[a] $C_{max:}$ maximum peak carbon of n-alkanes; [b] CPI_1: 1/2[$\Sigma C_{15–21}$ (odd carbon)/$\Sigma C_{14–20}$ (even carbon) + $\Sigma C_{15–21}$ (odd carbon)/$\Sigma C_{16–22}$ (even carbon)]; [c] CPI_2: 1/2[$\Sigma C_{25–35}$ (odd carbon)/$\Sigma C_{24–34}$ (even carbon) + $\Sigma C_{25–35}$ (odd carbon)/$\Sigma C_{26–36}$ (even carbon)]; [d] Alkterr: (C_{27} + C_{29} + C_{31} + C_{33})/$\Sigma C_{14–38}$; [e] LMW/HMW: $\Sigma nC_{21\text{-}}/\Sigma nC_{22+}$; [f] $\delta^{13}C$ = $\delta^{13}C$ of chloroform asphalts.

Organisms have different carbon isotope compositions, and the $\delta^{13}C$ values range from −22‰ to −31‰ for C3 plants and from −10‰ to −16‰ for C4 plants [1,2]. HCO_3^- in lake water provides carbon for photosynthesis of aquatic plants, and, hence, they have high $\delta^{13}C$ values. The $\delta^{13}C$ of phytoplankton in warm seawater is close to −20‰, while that of phytoplankton in cold seawater is around −30‰ [1,3]. Seagrasses have $\delta^{13}C$ values ranging from −10‰ to −16‰, and marine algae have $\delta^{13}C$ values around −18‰ [4]. The carbon isotopic composition of non-marine aquatic plants and algae is generally in the range of −12‰ to −26‰ [5]. In general, high $\delta^{13}C$ values correspond to a warm period and low values to a cold period [6,7]. The $\delta^{13}C$ (PDB) of the chloroform asphalts of the samples from the C_2t, P_2x, P_2w, P_3w, and T_1b ranged from −29.52 to −27‰, −29.76 to −28.32‰, −30.14 to −23.93‰, −32.17 to −29.15‰, and −30.81 to approximately −29.28‰, respectively (Table 1 and Table S2, Figures 2 and 3).

The Pr/Ph ratio is a useful indicator of the oxidation-reduction conditions of the sediment environment [41–44]. The Pr/Ph values of the samples from the C_2t, P_2x, P_2w, P_3w, and T_1b ranged from 0.29 to 0.67, 0.57 to 0.67, 0.49 to 0.83, 0.56 to 0.8, and 0.67 to 0.74 (Table 1 and Table S2, Figures 2–4). B-carotene is the most prominent compound in the carbon skeleton of carotenoids preserved in lakes and highly restricted marine environments, and its higher content indicates a higher reduction in waters [45,46]. B-carotene was detected in only a few samples from the C_2t, with a highly variable content. The ratio of β-carotene/$\Sigma C_{12\text{-}35}$ values ranged from 0.56 to 2.7 and had a mean value of 1.42. The two samples from the P_2x contained β-carotene, with β-carotene/$\Sigma C_{12\text{-}35}$ values ranging from 1.0 to 3.85 and a mean value of 2.42. The mean values of β-carotene/$\Sigma C_{12\text{-}35}$ in the P_2x, P_2w, P_3w, and T_1b were 0.51, 0.64, and 0.42. (Table 1 and Table S2, Figures 2 and 3).

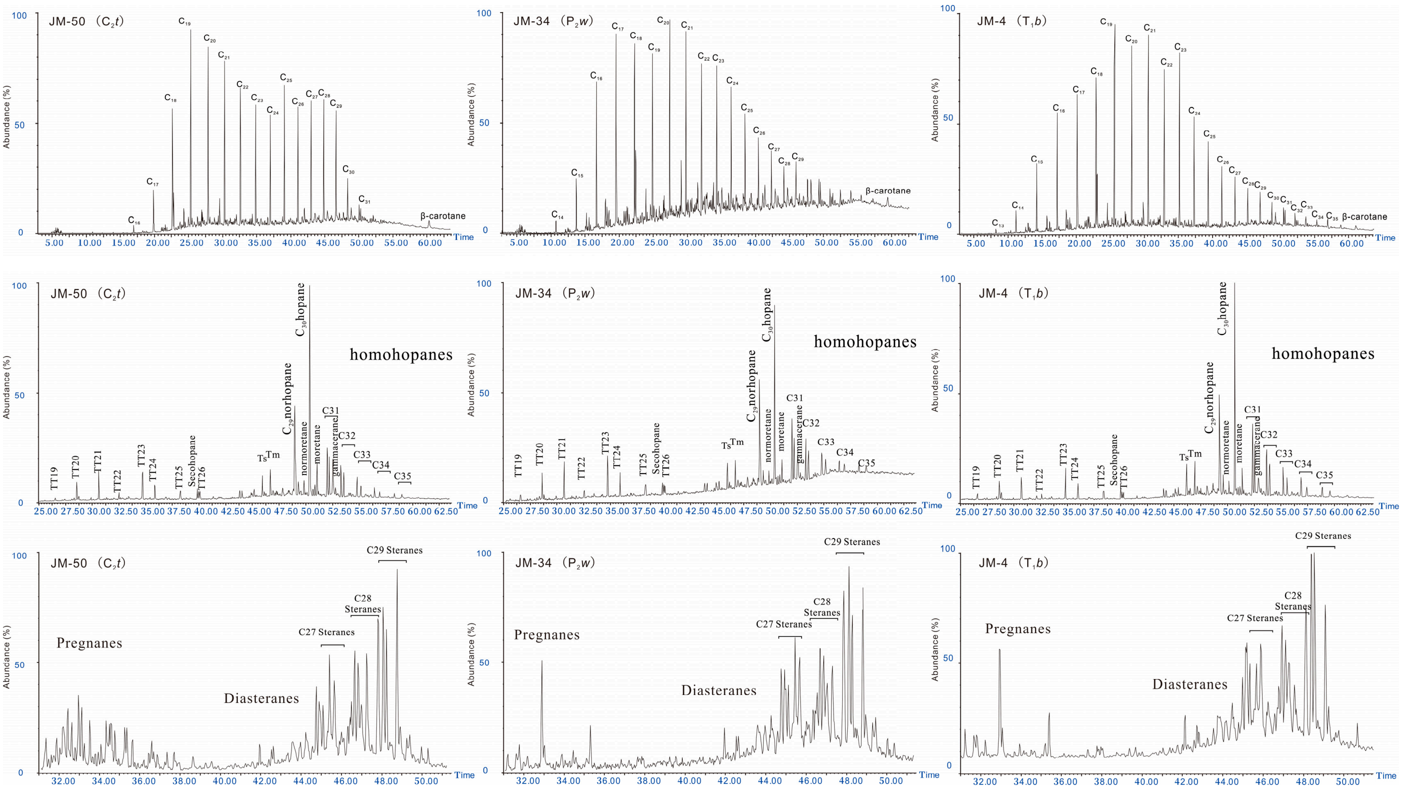

Figure 3. Chromatograms and mass fragmentogram of m/z = 191, 217, in the samples from MS-1 well of the Late Carboniferous–Early Triassic.

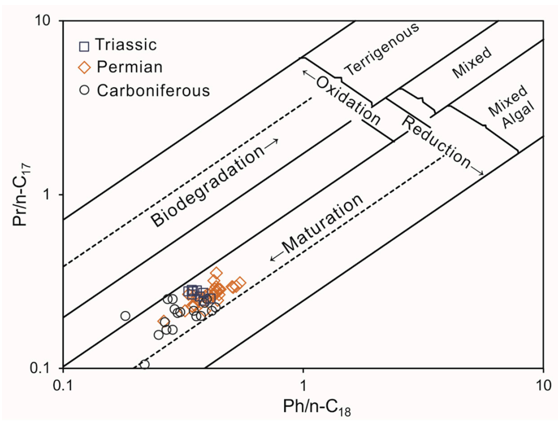

Figure 4. The correlation diagram of Ph/n-C_{18} and Pr/n-C_{17} in MS-1 well of the Late Carboniferous–Early Triassic.

4.2.2. Terpenoids and Steroids

Terpenes (including hopanes) are biomarker compounds, including tricyclic terpenes and pentacyclic triterpenes. The tricyclic terpenes of these samples in terms of tricyclic terpene abundance were distributed $C_{19} < C_{20} < C_{21} < C_{23}$ in an "ascending" pattern, and the tetracyclic C_{24} terpene abundance was higher. The C_{31}17β,21α(H)-hopane αβ-22S/(S + R) values for the C_2t, P_2x, P_2w, P_3w, and T_1b ranged from 0.38 to 0.67, 0.58 to 0.64, 0.51 to 0.64, 0.53 to 0.6, and 0.57 to 0.65 (Table 2). The values of C_{29}/C_{30}-hopane in the Carboniferous, Permian, and Triassic samples were 0.34–0.72, 0.43–0.89, and 0.42–0.82, respectively. Gammacerane is C_{30} pentacyclic triterpenoid, and high levels of gammacerane represent strongly reducing hypersaline environments [47–49], which were detected in all samples from the MS-1 well (Figure 3). The gammacerane indices (gammacerane/C_{31}-hopane) of the C_2t, P_2x, P_2w, P_3w, and T_1b ranged from 0.28 to 2.47, 0.51 to 0.73, 0.42 to

1.3, 0.21 to 0.67, and 0.21 to 0.83, respectively. The ratios of C_{27}-17α(H)-tridecane (Tm) to C_{27}-18α(H)-tridecane (Ts) effectively reflect the depositional environment and organic matter maturity [50–53]. Ts/Tm values in the Carboniferous, Permian, and Triassic samples ranged from 0.27 to 1.18, 0.28 to 0.91, and 0.22 to 0.79 (Tables 2 and S2, Figures 3 and 5). Steroids are another group of biomarker compounds, which are tetracyclic compounds with alkyl side chains, and the tetracyclic structures are collectively called steroid nuclei. The MS-1 well samples were rich in steroids, including C_{27}–C_{29} regular steroids and rearranged steroid series, mainly regular steroids (Figure 4). The C_{29}αααα-20S/20(S + R) values in the samples of C_2t, P_2x, P_2w, P_3w, and T_1b ranged from 0.19 to 0.49, 0.42 to 0.49, 0.42 to 0.52, 0.42 to 0.49, and 0.43 to 0.5, respectively, while the C_{29}-αββ/(αββ + αααα) values ranged from 0.23 to 0.51, 0.47 to 0.51, 0.44 to 0.53, 0.47 to 0.53, 0.47 to 0.53, and 0.47 to 0.57, respectively (Tables 2 and S2, Figures 3, 5 and 6).

Table 2. Parameters of hopane and sterane in Late Carboniferous–Early Triassic of MS-1 well.

Strata		C31αβ-22S/(S + R)	Gama [a]	C29/C30	Ts/Tm	C29-S [b]	C29-α [c]	ααα20R		
								C27	C28	C29
T_1b	Min.	0.57	0.21	0.42	0.22	0.43	0.47	11.37	19.33	43.04
	Max.	0.65	0.83	0.82	0.79	0.5	0.57	34.27	33.16	55.47
	Mean	0.59	0.41	0.63	0.54	0.46	0.53	27.5	21.15	50.57
P_3w	Min.	0.53	0.21	0.54	0.28	0.42	0.47	16.74	24.04	43.11
	Max.	0.6	0.67	0.89	0.69	0.49	0.53	27.4	32.35	55.28
	Mean	0.58	0.56	0.59	0.49	0.46	0.48	21.76	28.49	50.14
P_2w	Min.	0.51	0.42	0.48	0.35	0.42	0.44	22.47	23.25	40.79
	Max.	0.64	1.3	0.78	0.7	0.52	0.53	31.34	32.94	49.78
	Mean	0.57	0.51	0.68	0.53	0.46	0.51	27.44	26.52	46.87
P_2x	Min.	0.56	0.43	0.31	0.42	0.47	17.95	22.7	41.07	0.58
	Max.	0.61	0.76	0.89	0.49	0.51	34.92	30.91	52.75	0.64
	Mean	0.6	0.59	0.81	0.45	0.5	26.6	24.16	47.16	0.59
C_2t	Min.	0.38	0.28	0.34	0.27	0.19	0.23	18.25	17.76	37.14
	Max.	0.67	2.47	0.72	1.18	0.49	0.51	39.27	27.67	63.54
	Mean	0.585	0.635	0.57	0.725	0.43	0.45	28.92	23.63	46.57

[a] Gama. = gammacerane/C31-hopane. [b] C29-S = ααα-20S/20(S + R). [c] C29-α = C29[c]αββ/(αββ + ααα).

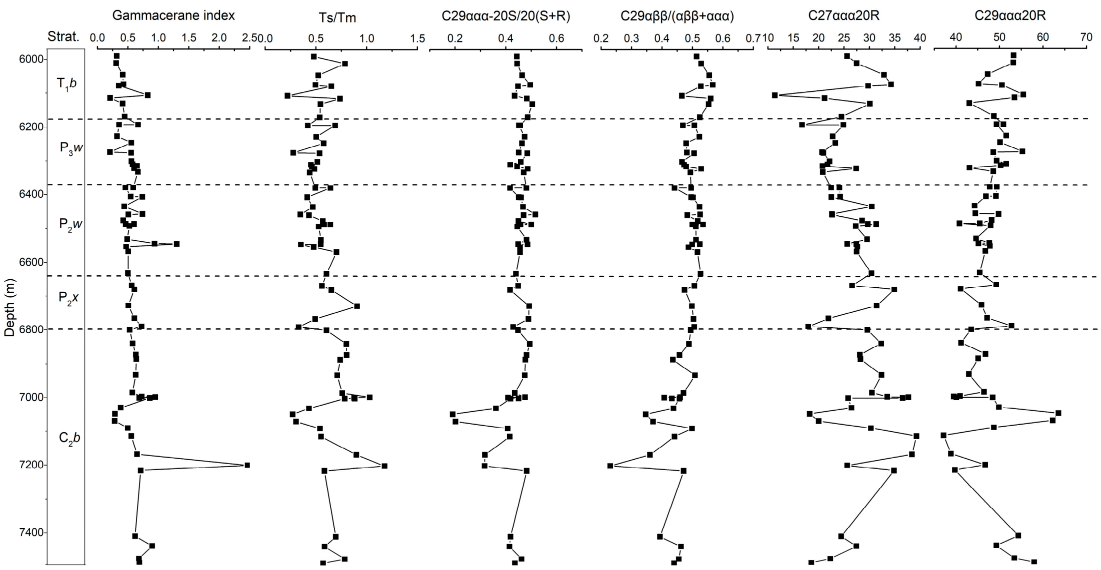

Figure 5. Profile for parameters from hopanoids and steranes of samples from the MS-1 well of the Late Carboniferous–Early Triassic.

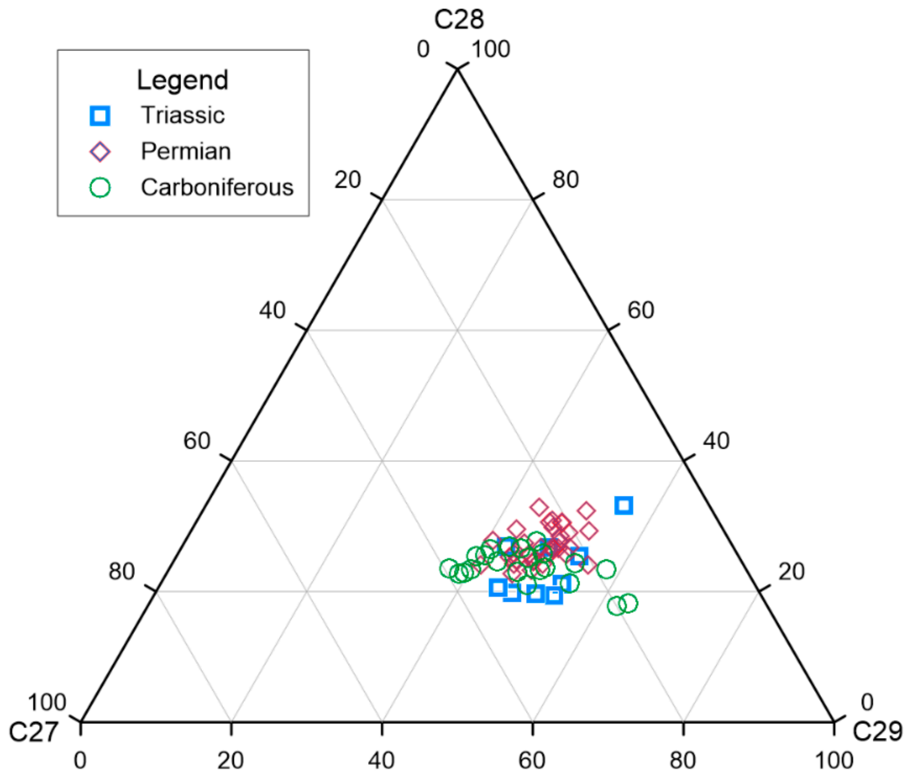

Figure 6. Ternary plot showing the distribution of regular steranes (C27–C28–C29) of samples from the MS-1 well of the Late Carboniferous–Early Triassic.

4.2.3. Organic Matter Maturity

The maximum pyrolysis temperature (T_{max}) in the Carboniferous samples from the MS-1 well was mainly 441–502 °C, indicating that the hydrocarbon source rocks are in the stage of high maturity–overmaturity evolution. T_{max} values of 425–468 °C for hydrocarbon source rocks of the Xiazijie Formation from the Permian indicated that these rocks have also reached a high-maturity evolutionary stage. The samples from the Lower Permian Urho Formation had a T_{max} range of 425–471 °C, which shows that the hydrocarbon source rocks have reached the mature–high-maturity evolutionary stage. The samples from the Urho Formation of the Upper Permian also showed a mature evolutionary stage with T_{max} values of 428–443 °C. The T_{max} values of the Baikouquan Formation of the Triassic were mainly 430–441 °C, indicating that these rocks have just entered the mature evolutionary stage (Table 1, Figure 2).

Biomarker compound parameters are another tool for evaluating the maturity of organic matter in sedimental rocks [51,54,55]. During the heating of hopanes and steranes under geological conditions, the R conformation is converted to the S conformation, forming a mixed conformation of R + S. In general, a higher 22S/(S + R) ratio represents higher maturity [52]. In addition, $C_{29}\alpha\beta\beta$ has higher stability than $C_{29}\alpha\alpha\alpha$, and the value of C_{29} $\alpha\beta\beta/(\alpha\alpha\alpha\alpha + \alpha\beta\beta)$ increases abruptly in the first half of a raw oil zone. The C_{31}17β, 21α(H)-hopane, and 31αβ-22S/(S + R) values, sterane $C_{29}\alpha\alpha\alpha$-20S/20(S + R) values, and C_{29}-$\alpha\beta\beta/(\alpha\beta\beta + \alpha\alpha\alpha\alpha)$ values from the MS-1 well all indicated that the Late Carboniferous–Early Triassic organic matter of MS-1 has reached the mature stage in general.

In general, the ratio of C_{27}-17α(H)-triacontane (Tm) to C_{27}-18α(H)-triacontane (Ts) can effectively reflect the organic matter maturity and depositional environment, and, in the post-rock stage, C_{27}-17α(H)-trisnorhopane (Tm) is less stable than C_{27}-18α(H)-trisnorhopane (Ts), and, as the maturity of crude oil increases, the Ts/Tm values also increase with increasing maturity of crude oil. and for immature samples. The Ts/Tm values of samples from the C_2t similarly indicated that the organic matter has reached the maturity stage. Ts/Tm can also reflect the redox conditions of the depositional environment, with low Ts/Tm values for oxidizing environments and high values for reducing environments [52]; however, the samples from the MS-1well did not exhibit significant environmental indicator features.

The Rock-Eval indicated that the organic matter of the MS-1 well is in the mature stage, but did not show an increase in the parameters of organic matter maturity with increasing depth of the formation. Ts/Tm, $C_{29}\alpha\alpha\alpha\alpha$-20S/20(S + R), and C_{29}-$\alpha\beta\beta/(\alpha\beta\beta + \alpha\alpha\alpha\alpha)$ even showed a decreasing trend with organic matter type and depositional environment, indicating that the biomarkers in the study area are not significantly affected by maturity, and, on the other hand, supporting that MS-1 organic geochemical parameters can be used to reconstruct the paleoclimate and paleoenvironment.

5. Sedimentary Environment

5.1. Carboniferous

The Telegula Formation (C_2t)

The C_2t stratigraphic logs can be divided into three lithologic zones (Figures 1 and 7): the depth of 6806.0–6952.0 m is mainly gray-brown, conglomeratic mudstone with gray, conglomeratic mud siltstone in unequal thickness interbedded and gray tuff with tuff siltstone interbedded; the depth of 6952.0–7265.0 m is dominated by gray and greenish-gray tuff, interbedded with black coal, gray-black sunken tuff, tuffaceous mudstone, and andesite; and the depth of 7265.0–7500.0 m is dominated by gray, dark-gray, and gray-black tuffs, interbedded with gray-black tuffaceous siltstone. The lithologic assemblage indicates that the C_2t was frequently volcanic, the climate was relatively warm and humid, terrestrial higher plants were relatively developed, and large amounts of terrestrial organic matter were usually deposited in nearshore or shallow water along with tuffaceous debris. $C_{29}\alpha\alpha\alpha\alpha$20R and isotopes of organic matter (−29.52 to −27‰) also indicated a high content of terrestrial organic matter mixed with mixed aquatic plants in the sediments of the MS-1 well during this period. Meanwhile, the abundance of short-chain carbon number n-alkanes, Pr/Ph, and gammacerane indices indicates high salinity and reduction in the water column [52]. Additionally, intermittent volcanic activities can carry the terrestrial organic matter to the water column, causing a dramatic increase in organic matter and a rise in the salinity and reducibility of the water column [56]. In terms of biomarker trends, the aquatic life content tends to increase while the salinity and oxidation of the water column increases. Considering that the geochemistry of the Carboniferous volcanic rocks of the MS-1 well shows an island arc setting, while the complete closure of the western ocean of the Junggar Basin was delayed until the Early Permian, we believe that the MS-1 well was in a relatively closed residual sea environment, and the relatively humid climate made terrestrial plants flourish. Two recessions and one flooding event can be identified by the chloroform asphalts of δ^{13}C (PDB), showing two decreasing trends of δ^{13}C and an abrupt rise at 7300 m depth.

5.2. Permian

5.2.1. The Xiazijie Formation (P_2x)

The P_2x is directly unconformable, overlying the Carboniferous (Figures 1 and 7); 6641.0–6655.0 m is a set of dark-gray mudstone. It is mainly gray-white, muddy siltstone from the depth of 6655.0 to 6700.0 m, interbedded with gray mudstone and siltstone; an area of gray-white, muddy siltstone from the depth of 6700.0 to 6800.0 m, interbedded with gray mudstone and siltstone with varying thickness; and gray, gravelly siltstone from a depth of 6800.0 to 6806.0 m. The lithology of the P_2x period is typical of lacustrine sedimentation. Since the stratigraphy of the Fengcheng Formation is missing [57–59], we speculate that the super-lake basin of the Fengcheng Formation gradually shrunk with stratigraphic uplift, and the P_2x turned into a period of subsidence. During P_2x, several alluvial fans developed in the western part of the Junggar Basin, and the sediments were characterized by coarse-grained sandstone and conglomerate. The Mosuowan area served as the sedimentary center, and the gray, fine sandstone and mudstone were mainly deposited there. Biomarkers and $\delta^{13}C$ (PDB) of the chloroform asphalts (−29.76 to −28.32‰) indicated a sustained increase in aquatic life content, a decrease in water column salinity, and an increase in water column oxidation.

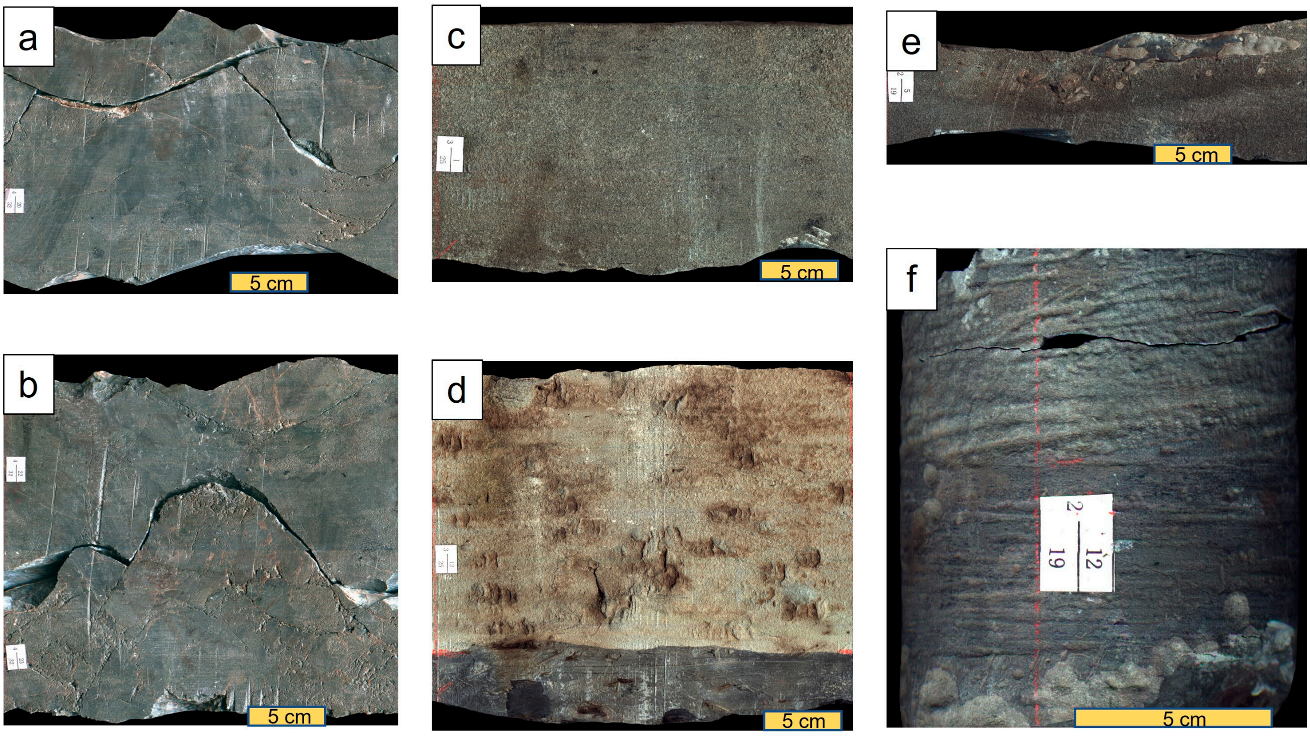

Figure 7. Scanning core photos of samples from the MS-1 well: (**a**,**b**), tuff in C_2t; (**c**), siltstone mudstone in P_2w; (**d**), grayish-white siltstone and black mudstone in P_3w, with scouring surface between them; (**e**,**f**), siltstone mudstone in T_1b.

5.2.2. The Lower and Upper Urho Formation (P_2w, P_3w)

The lithology of the Middle Permian–Upper Permian Urho Formation (Lower and Upper Urho Formation) is characterized as follows (Figures 1 and 7): It consists of grayish-white siltstone, muddy siltstone, and conglomeratic siltstone, interbedded with grayish-brown, brownish-gray, gray, and greenish-gray mudstone, platy mudstone, and siltstone; from the depth of 6455.0–6548.0 m, it consists of greenish-gray, gray, brownish-gray, and dark-gray mudstone and siltstone, interbedded with grayish-white and muddy siltstone and siltstone; from 6548.0 to 6641.0 m, it consists of gray siltstone, muddy siltstone, and conglomeratic siltstone, interbedded with gray and dark-gray mudstone and siltstone; an interval (depth of 6178.0–6256.0 m) consists of brownish-gray, grayish-brown, beige, and gray, muddy siltstone, siltstone, and conglomerate, interbedded with brownish-gray and grayish-brown mudstone in unequal thickness; and the depth of 6256.0–6374.0 m is gray siltstone, sandstone, and muddy siltstone, interbedded with brownish-gray, grayish-brown, brown mudstone, and silt mudstone. The lithological assemblage of the P_2w and P_3w is a deltaic foreland deposit. Combined with geochemical indicators, it shows an overall lake retreat process with a continuous increase in terrestrial organic matter content and small changes in water salinity and reducibility. The $\delta^{13}C$ (PDB) of the chloroform asphalts at P_2w ranged from −30.14 to −23.93‰, during which the maximum flooding surface occurred with $\delta^{13}C$ reaching −24‰. In contrast, P_3w had the largest lake retreat event during C_2t–T_1b, reflecting the climate transition from wet to dry. β-carotene/$\Sigma C_{12\text{-}35}$ showed that the salinity of P_3w was higher than that of P_2w, which might have been caused by the repeated lake level fluctuations.

5.2.3. The Baikouquan Formation (T_1b)

The lithology of T_1b is divided into two sections (Figures 1 and 7), the first section (depth of 5939.0–5991.0 m) is gray, brownish-gray, off-white, muddy siltstone, siltstone, sand conglomerate, and gravelly, fine sandstone interbedded with brownish-gray, gray mudstone, and coarse siltstone, while the second section (depth of 5991.0–6178.0 m) is brownish-gray, off-white, gray, muddy siltstone, siltstone, gravelly, muddy siltstone, conglomeratic siltstone, and sand conglomerate, interbedded with gray and brown-gray mudstone. The lithologic assemblage of the T_1b is braided river deltaic sedimentation with migration of deposition centers of the lake basin and reduced water salinity. A transient flooding event was found in the middle of the Baikouquan Formation, which increased the organic matter content of terrestrial sources and increased water salinity. The $\delta^{13}C$ (PDB) of the chloroform asphalts ranged from −30.81 to −29.28‰, with obvious higher plant carbon isotope characteristics. Pr/Ph had been increasing continuously since P_3w and reached its highest point, indicating a significant change in the depositional environment invention, i.e., from shallow lakeside to braided river deposition.

6. Global Tectonics and Environmental Change Drives

Large-scale sea retreat events during the Carboniferous period exposed the seafloor at the land margin, expanded the land area globally, and created fertile swamps and wetlands as freshwater rivers flowed through the new continental mass [57,60,61]. At the same time, the warm and humid climate made Lycopodium grow densely, and the tall ferns provided raw materials for coal formation, and the European continent and Siberia in the north, as well as the land of north China, which are the major coal-gathering areas in the world [62]. The C_2t coal formation and higher, plant-rich tuffs drilled in the Carboniferous MS-1 well also reflect the global climatic characteristics of this period, but the strong volcanic activity in the Late Carboniferous Junggar Basin may have affected the growth of Carboniferous fern plants and, thus, the regional development of the coal formation. The most important global event of the Permian was the Permian–Triassic extinction that occurred at the end of the Permian, an extinction event that can be divided into one to three stages [61,63–65]. The first mini-peak may have been due to a gradual change in the environment due to sea level changes, oceanic hypoxia, and the arid climate due to the formation of the Pangaea continent. The later peaks were rapid and dramatic, probably due to impact events, super volcanic eruptions, or abrupt sea level changes that caused a massive release of methane hydrates that lasted about 60,000 years [65–67]. However, this event has no obvious carbonate record in the Junggar Basin. Since the Permian sediments of the MS-1 well are dominated by terrestrial organic matter, the negative organic carbon isotope drift is not significant. The core samples show that the Urho Formation samples are darker in color than the Baikouquan Formation, indicating that its depositional environment may have dealt with a global anoxic background. Influenced by the global aridification triggered by the Pangaea, the drought in the Junggar Basin reached its peak in the Late Permian–Early Triassic. The drought in Junggar began in the Middle Permian, and the lakes on the southern edge of Junggar dried up in its late stage, with evaporation exceeding recharge, and the lake extent south of Karameri in the Early Triassic also gradually decreased until it was replaced by the red layer, further confirming the persistence and development of the arid climate, a fact also illustrated by the gradual increase in the oxidation of the sedimentary environment of the MS-1 well (Figure 8).

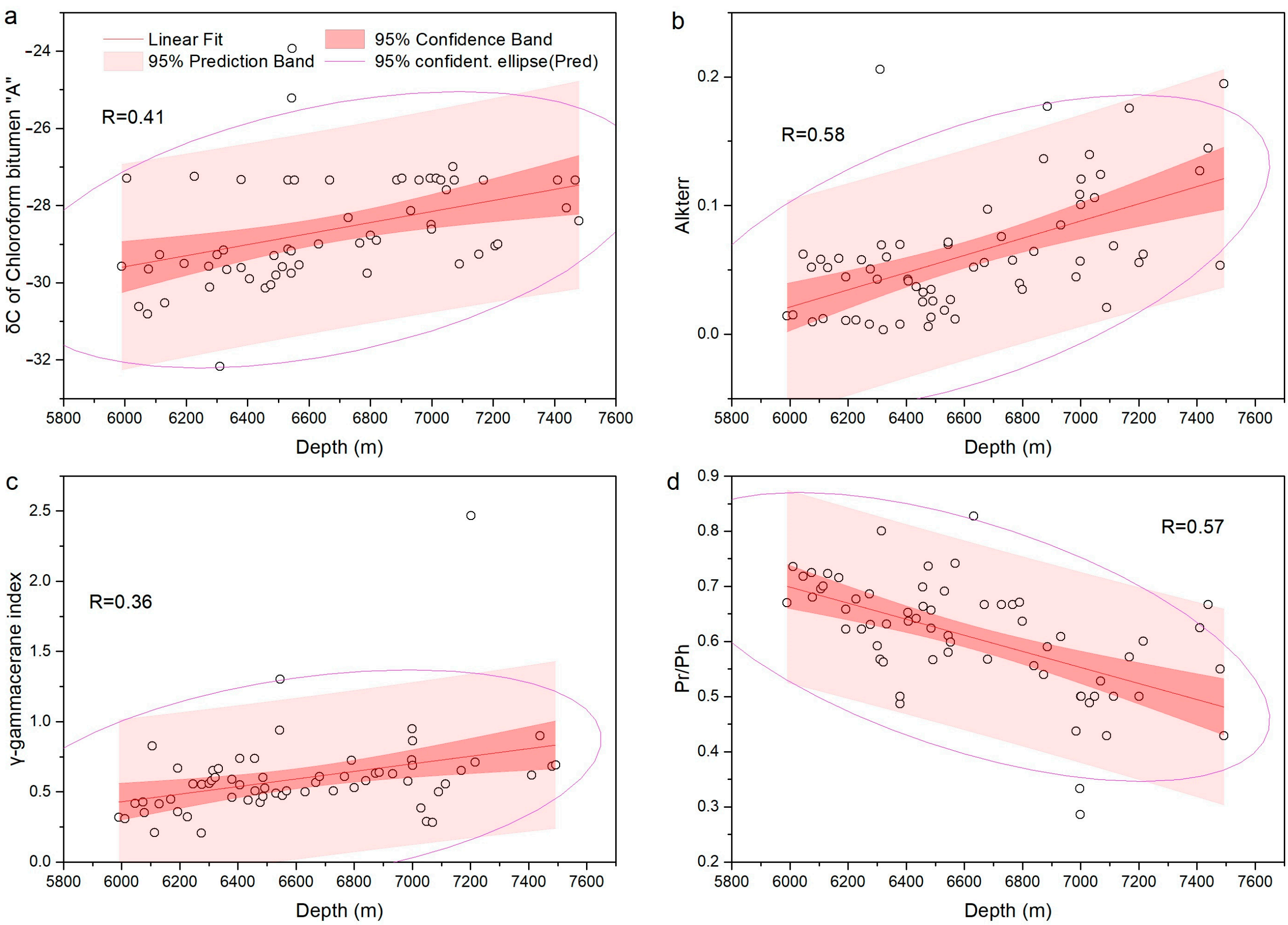

Figure 8. Correlation between depth and δC of chloroform bitumen "A" (**a**), Alkterr (**b**), γ-gammacerane index (**c**), Pr/Ph (**d**).

The Late Paleozoic orogenic belt in northern Xinjiang and adjacent areas developed a series of successive, southward accretionary belts along the broad South Siberian active margin, forming the Alaska–Aleutian arc system (Kokchetav–Morth Tianshan), the Japanese arc system (Altai, Chinese Middle Tianshan), and the Mariana arc system (Balkhash, West Junggar, East Junggar) [4,9] (Figure 9). Paleomagnetic reconstructions indicate that complex nappes occurred in the Early Paleozoic. In the Late Devonian, a complex Kokchetav–North Tianshan arc system with a straight extension of the main axis was formed under growth and fusion of the circum-microcontinental type. Approximately corresponding to the late Early Carboniferous, the Junggar paleo sheet formed a rift trough along the Bogda area, separating the Junggar-occupied sheet. The rift trough did not reach the level of the emergence of oceanic crust, so it is also called the Ora Valley. After the middle of the Early Carboniferous, the Siberian plate and the Junggar paleolithic sheet underwent continental collisional orogeny, and the ocean basin disappeared. The ocean between the Junggar paleo sheet and Kazakhstan finally closed at the end of the Carboniferous or the beginning of the Permian, while the ocean south of the basin closed in the Late Carboniferous and entered the intra-land orogenic stage, and the relatively closed residual marine environment in the Late Carboniferous study area coincided with it. In the Permian period, geosyncline closed, and folded mountain series were formed successively, and the paleo-plates were gradually linked to form a joint paleo-continent (Pangaea). With the further expansion of the land area, gymnosperms began to decline on land, true and seed ferns flourished, and the first gymnosperms appeared. From the Permian to the Middle Triassic, the Junggar Basin was in the foreland basin tectonic development stage, and the sediment evolution of the Xiazijie, Urho, and Baikouquan Formations also reflected the gradual disappearance of marine fingerprints and the increasingly obvious characteristics of continental sedimentation; the organic matter of terrestrial origin continued to increase, and the salinity of water bodies became increasingly low. In conclusion, regional tectonic evolution constrained the variability of lake waters in the MS-1 well, while the Carboniferous global warming and wetting event, Permian anoxic event, and Late Permian–Early Triassic drought event influenced the organic matter composition and redox conditions of the lake waters.

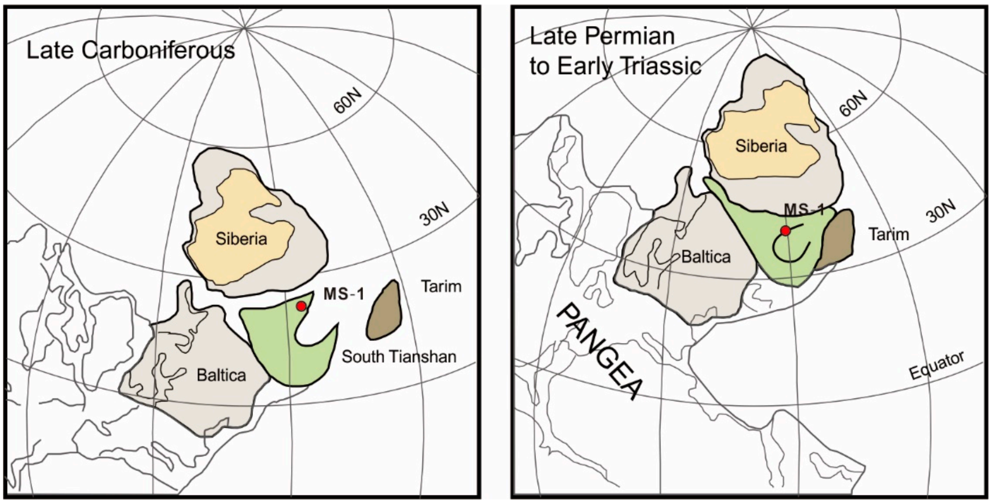

Figure 9. Paleogeographic reconstruction for the bending of the Kazakhstan oroclines. Modified after [68,69].

7. Conclusions

The organic carbon content in the Carboniferous–Lower Permian sedimentary rocks drilled from MS-1 in the Mosuowan area of the Junggar Basin is low, but the Carboniferous tuffs and coal-bearing rocks are high in organic matter and have potential hydrocarbon generation capabilities. The organic matter evolution is all at a mature stage, but biomarker parameters were not significantly subjected to thermal evolution. During the Late Carboniferous, the Mosuowan area was located in a relatively enclosed remnant marine environment with a relatively humid climate that allowed for vigorous terrestrial vegetation, abundant rivers flowing into the water, and reduced water salinity yet increased depth. The Xiazijie Formation of the Middle Permian was a period of basin subsidence during which the basin area expanded significantly, and organic geochemical information indicates a continuous increase in aquatic organisms, a decrease in lake water salinity, and an increase in water oxidation. The lithologic assemblage of the Urho Formation in Permian was developed on the deltaic foreland. The biomarkers and isotopes of organic matter show an overall lake retreat process with a continuous increase in terrestrial organic matter and little change in water salinity and reduction, during which significant flooding events showed a significant decrease in terrestrial organic matter, an increase in aquatic organisms, and an increase in water salinity and reduction. The Baikouquan Formation of the Early Triassic was deposited as a braided river delta, with a migration of deposition centers of the lake basin and a decrease in water salinity, during which there was a brief flooding event, an increase in organic matter of terrestrial origin, and an increase in water salinity. Paleo-Asian ocean subduction and continental collision constrained the changes of waters in the MS-1 well during the Late Carboniferous–Early Permian, while the continuous increase in sediment, terrestrial organic matter, water desalination, and oxidation enrichment in the Mosuowan area, and the global warming and wetting events of the Carboniferous, Permian anoxic events, and Late Permian–Early Triassic drought events affected the lipid biomarkers and stable isotopes of the organic matter composition; however, the P–T biological mass extinction events were not clearly recorded.

Supplementary Materials: The following are available online at https://www.mdpi.com/article/10.3390/min12101299/s1, Table S1: TOC and rock pyrolysis parameters of the Late Carboniferous-Early Triassic rocks in MS-1 well, Table S2: Parameters of δ^{13C} values of n-alkanes, Pr, Ph, β-carotene and chloroform extracts from MS1 wells of the Late Carboniferous-Early, Table S3: Parameters of hopance and sterane in Late Carboniferous-Early Triassic of MS1 well.

Author Contributions: Conceptualization: S.Z. (Shuncun Zhang). Data curation: T.W. and H.G. Investigation: T.W., H.G. and S.Z. (Shengyin Zhang). Methodology: B.C. Writing—original draft: S.Z. (Shuncun Zhang). Writing—review and editing: S.Z. (Shengyin Zhang). All authors have read and agreed to the published version of the manuscript.

Funding: This study was financially supported by the Guangxi Natural Science Foundation, China (2020GXNSFBA297128); the Special Talent Project of Guangxi Science and Technology Base, China (Guike AD20238041); the National Natural Science Foundation of China (grant no. 41872145).

Institutional Review Board Statement: Not applicable.

Informed Consent Statement: Not applicable.

Data Availability Statement: The data are contained within the article.

Conflicts of Interest: The authors declare no conflict of interest.

References

1. Shen, S.Z.; Shi, G.R. Late Paleozoic deep Gondwana and its peripheries: Stratigraphy, biological events, paleoclimate and paleogeography. *Gondwana Res.* **2013**, *24*, 1–4. [CrossRef]
2. Feng, Y.; Song, H.J.; Bond, D.P.G. Size variations in foraminifers from the early Permian to the Late Triassic: Implications for the Guadalupian-Lopingian and the Permian-Triassic mass extinctions. *Paleobiology* **2020**, *46*, 511–532. [CrossRef]
3. Wang, Y.J.; Jia, D.; Pan, J.G.; Wei, D.T.; Tang, Y.; Wang, G.D.; Wei, C.R.; Ma, D.L. Multiple-phase tectonic superposition and reworking in the Junggar Basin of northwestern China-Implications for deep-seated petroleum exploration. *Aapg Bull.* **2018**, *102*, 1489–1521. [CrossRef]
4. Xiao, W.J.; Windley, B.F.; Allen, M.B.; Han, C.M. Paleozoic multiple accretionary and collisional tectonics of the Chinese Tianshan orogenic collage. *Gondwana Res.* **2013**, *23*, 1316–1341. [CrossRef]
5. Ju, W.; Hou, G.T.; Li, L.; Xiao, F.F. End Late Paleozoic tectonic stress field in the southern edge of Junggar Basin. *Geosci. Front.* **2012**, *3*, 707–715. [CrossRef]
6. Hendrix, M.S.; Brassell, S.C.; Carroll, A.R.; Graham, S.A. Sedimentology, organic geochemistry, and petroleum potential of Jurassic coal measures: Tarim, Junggar, and Turpan basins, northwest China. *Aapg Bull.-Am. Assoc. Pet. Geol.* **1995**, *79*, 929–959.
7. Xiao, M.; Wu, S.T.; Yuan, X.J.; Cao, Z.L.; Xie, Z.R. Diagenesis effects on the conglomerate reservoir quality of the Baikouquan Formation, Junggar Basin, China. *J. Pet. Sci. Eng.* **2020**, *195*, 17. [CrossRef]
8. Han, Y.G.; Zhao, G.C. Final amalgamation of the Tianshan and Junggar orogenic collage in the southwestern Central Asian Orogenic Belt: Constraints on the closure of the Paleo-Asian Ocean. *Earth-Sci. Rev.* **2018**, *186*, 129–152. [CrossRef]
9. Xiao, W.J.; Windley, B.F.; Han, C.M.; Liu, W.; Wan, B.; Zhang, J.; Ao, S.J.; Zhang, Z.Y.; Song, D.F. Late Paleozoic to early Triassic multiple roll-back and oroclinal bending of the Mongolia collage in Central Asia. *Earth-Sci. Rev.* **2018**, *186*, 94–128. [CrossRef]
10. Han, B.F.; Ji, J.Q.; Song, B.; Chen, L.H.; Zhang, L. Late Paleozoic vertical growth of continental crust around the Junggar Basin, Xinjiang, China (Part I): Timing of post-collisional plutonism. *Acta Petrol. Sin.* **2006**, *22*, 1077–1086.
11. Yu, K.H.; Cao, Y.C.; Qiu, L.W.; Sun, P.P.; Jia, X.Y.; Wan, M. Geochemical characteristics and origin of sodium carbonates in a closed alkaline basin: The Lower Permian Fengcheng Formation in the Mahu Sag, northwestern Junggar Basin, China. *Palaeogeogr. Palaeoclimatol. Palaeoecol.* **2018**, *511*, 506–531. [CrossRef]
12. Yang, W.; Feng, Q.A.; Liu, Y.Q.; Tabor, N.; Miggins, D.; Crowley, J.L.; Lin, J.Y.; Thomas, S. Depositional environments and cyclo- and chronostratigraphy of uppermost Carboniferous-Lower Triassic fluvial-lacustrine deposits, southern Bogda Mountains, NW China-A terrestrial paleoclimatic record of mid-latitude NE Pangea. *Glob. Planet. Chang.* **2010**, *73*, 15–113. [CrossRef]
13. Metcalfe, I.; Foster, C.B.; Afonin, S.A.; Nicoll, R.S.; Mundil, R.; Wang, X.F.; Lucas, S.G. Stratigraphy, biostratigraphy and C-isotopes of the Permian-Triassic non-marine sequence at Dalongkou and Lucaogou, Xinjiang Province, China. *J. Asian Earth Sci.* **2009**, *36*, 503–520. [CrossRef]
14. Gastaldo, R.A.; Neveling, J.; Clark, C.K.; Newbury, S.S. The terrestrial Permian-Triassic boundary event bed is a nonevent. *Geology* **2009**, *37*, 199–202. [CrossRef]
15. Meng, Z.Y.; Liu, Y.Q.; Jiao, X.; Ma, L.T.; Zhou, D.W.; Li, H.; Cao, Q.; Zhao, M.R.; Yang, Y.Y. Petrological and organic geochemical characteristics of the Permian Lucaogou Formation in the Jimsar Sag, Junggar Basin, NW China: Implications on the relationship between hydrocarbon accumulation and volcanic-hydrothermal activities. *J. Pet. Sci. Eng.* **2022**, *210*, 17. [CrossRef]
16. Hu, D.; Rao, S.; Wang, Z.T.; Hu, S.B. Thermal and maturation history for Carboniferous source rocks in the Junggar Basin, Northwest China: Implications for hydrocarbon exploration. *Pet. Sci.* **2020**, *17*, 36–50. [CrossRef]

17. Feng, M.Y.; Liu, T.; Lin, T.; Liu, X.H.; Li, N.X.; Xi, A.H. Fracture Fillings and Implication of Fluid Activities in Volcanic Rocks: Dixi Area in Kelameili Gas Field, Junggar Basin, Northwestern China. *Minerals* **2019**, *9*, 154. [CrossRef]
18. Liu, B.B.; Tan, C.P.; Yu, X.H.; Qu, J.H.; Zhao, X.M.; Zhang, L. Sedimentary characteristics and controls of a retreating, coarse-grained fan-delta system in the Lower Triassic, Mahu Depression, northwestern China. *Geol. J.* **2019**, *54*, 1141–1159. [CrossRef]
19. Zhang, M.M.; Liu, Z.J.; Qiu, H.J.; Xu, Y.B. Characteristics of organic matter of oil shale in the sequence stratigraphic framework at the northern foot of Bogda Mountain, China. *Oil Shale* **2016**, *33*, 31–44. [CrossRef]
20. Jiao, Y.Q.; Yan, J.X.; Li, S.T.; Yang, R.Q.; Lang, F.J.; Yang, S.K. Architectural units and heterogeneity of channel reservoirs in the Karamay formation, outcrop area of Karamay oil field, Junggar basin, northwest China. *Aapg Bull.* **2005**, *89*, 529–545. [CrossRef]
21. Wilhem, C.; Windley, B.F.; Stampfli, G.M. The Altaids of Central Asia: A tectonic and evolutionary innovative review. *Earth-Sci. Rev.* **2012**, *113*, 303–341. [CrossRef]
22. Allen, M.B.; Windley, B.F.; Chi, Z. Palaeozoic collisional tectonics and magmatism of the Chinese Tien Shan, central Asia. *Tectonophysics* **1993**, *220*, 89–115. [CrossRef]
23. Liu, X.J.; Xiao, W.J.; Xu, J.F.; Castillo, P.R.; Shi, Y. Geochemical signature and rock associations of ocean ridge-subduction: Evidence from the Karamaili Paleo-Asian ophiolite in east Junggar, NW China. *Gondwana Res.* **2017**, *48*, 34–49. [CrossRef]
24. Bai, J.K.; Chen, J.L.; Yan, Z.; Tang, Z.; Xu, X.Y.; Li, J.L. The timing of opening and closure of the Mayile oceanic basin: Evidence from the angular unconformity between the Middle Devonian and its underlying geological body in the southern West Junggar. *Acta Petrol. Sin.* **2015**, *31*, 133–142.
25. Sengor, A.M.C.; Natal'In, B.A.; Sunal, G.; van der Voo, R. A new look at the altaids: A superorogenic complex in northern and central asia as a factory of continental crust. part I: Geological data compilation (exclusive of palaeomagnetic observations). *Austrian J. Earth Sci.* **2014**, *107*, 169–232.
26. Weng, K.; Xu, X.Y.; Ma, Z.P.; Chen, J.L.; Sun, J.M.; Zhang, X. The geochemistry and chronology characteristics and the geological significance of ultramafic rock in Mayile ophiolite, West Junggar, Xinjiang. *Acta Petrol. Sin.* **2016**, *32*, 1420–1436.
27. Chen, S.; Guo, Z.J. Time constraints, tectonic setting of Dalabute ophiolitic complex and its significance for Late Paleozoic tectonic evolution in West Junggar. *Acta Petrol. Sin.* **2010**, *26*, 2336–2344.
28. Xu, X.; Zhou, K.F.; Wang, Y. Study on extinction of the remnant oceanic basin and tectonic setting of West Junggar during Late Paleozoic. *Acta Petrol. Sin.* **2010**, *26*, 3206–3214.
29. Zhang, M.; Wang, G.C.; Zhang, X.H.; Liao, Q.A.; Wang, W.; Guo, R.L.; Zhang, P. Reconstruction of the Silurian to Devonian stratigraphic succession along the northeastern margin of the Junggar block, Xinjiang, NW China, and its tectono-paleogeographic implications for the southwestern Central Asian Orogenic Belt. *Sediment. Geol.* **2021**, *411*, 23. [CrossRef]
30. Novikov, I.S. Reconstructing the stages of orogeny around the Junggar basin from the lithostratigraphy of Late Paleozoic, Mesozoic, and Cenozoic sediments. *Russ. Geol. Geophys.* **2013**, *54*, 138–152. [CrossRef]
31. He, D.F.; Li, D.; Fan, C.; Yang, X.F. Geochronology, geochemistry and tectonostratigraphy of Carboniferous strata of the deepest Well Moshen-1 in the Junggar Basin, northwest China: Insights into the continental growth of Central Asia. *Gondwana Res.* **2013**, *24*, 560–577. [CrossRef]
32. Ji, Y.L.; Zhou, Y.; Kuang, J.; Wan, L.; Zhang, R.; Lu, C.H. The formation and evolution of Chepaizi-Mosuowan paleo-uplift and its control on the distributions of sedimentary facies in the Junggar Basin. *Sci. China-Earth Sci.* **2010**, *53*, 818–831. [CrossRef]
33. Shi, Y.Q.; Ji, H.C.; Yu, J.W.; Xiang, P.F.; Yang, Z.B.; Liu, D.D. Provenance and sedimentary evolution from the Middle Permian to Early Triassic around the Bogda Mountain, NW China: A tectonic inversion responding to the consolidation of Pangea. *Mar. Pet. Geol.* **2020**, *114*, 104–169. [CrossRef]
34. Zhang, Z.H.; Qin, L.M.; Qiu, N.S.; Zhong, N.N.; Zhang, Z.Y.; Li, W. Combination and superimposition of source kitchens and their effects on hydrocarbon accumulation in the hinterland of the Junggar Basin, west China. *Pet. Sci.* **2010**, *7*, 59–72. [CrossRef]
35. Qiu, N.S.; Ming, Z.; Wang, X.L.; Yang, H.B. Tectono-thermal evolution of the Junggar Basin, NW China: Constraints from R-o and apatite fission track modelling. *Pet. Geosci.* **2005**, *11*, 361–372.
36. Peters, K.E. Guidelines for evaluating petroleum source rock using programmed pyrolysis. *Aapg Bull.-Am. Assoc. Pet. Geol.* **1986**, *70*, 318–329.
37. Bray, E.; Evans, E. Distribution of n-paraffins as a clue to recognition of source beds. *Geochim. Et Cosmochim. Acta* **1961**, *22*, 2–15. [CrossRef]
38. Cheng, B.; Xu, J.B.; Lu, Z.Q.; Li, Y.H.; Wang, W.C.; Yang, S.; Liu, H.; Wang, T.; Liao, Z.W. Hydrocarbon source for oil and gas indication associated with gas hydrate and its significance in the Qilian Mountain permafrost, Qinghai, Northwest China. *Mar. Pet. Geol.* **2018**, *89*, 202–215. [CrossRef]
39. Herrera-Herrera, A.V.; Mallol, C. Quantification of lipid biomarkers in sedimentary contexts: Comparing different calibration methods. *Org. Geochem.* **2018**, *125*, 152–160. [CrossRef]
40. Silliman, J.E.; Schelske, C.L. Saturated hydrocarbons in the sediments of Lake Apopka, Florida. *Org. Geochem.* **2003**, *34*, 253–260. [CrossRef]
41. Holtvoeth, J.; Whiteside, J.H.; Engels, S.; Freitas, F.S.; Grice, K.; Greenwood, P.; Johnson, S.; Kendall, I.; Lengger, S.K.; Lucke, A.; et al. The paleolimnologist's guide to compound-specific stable isotope analysis-An introduction to principles and applications of CSIA for Quaternary lake sediments. *Quat. Sci. Rev.* **2019**, *207*, 101–133. [CrossRef]
42. Schinteie, R.; Brocks, J.J. Paleoecology of Neoproterozoic hypersaline environments: Biomarker evidence for haloarchaea, methanogens, and cyanobacteria. *Geobiology* **2017**, *15*, 641–663. [CrossRef]

43. Tulipani, S.; Grice, K.; Greenwood, P.F.; Haines, P.W.; Sauer, P.E.; Schimmelmann, A.; Summons, R.E.; Foster, C.B.; Bottcher, M.E.; Playton, T.; et al. Changes of palaeoenvironmental conditions recorded in Late Devonian reef systems from the Canning Basin, Western Australia: A biomarker and stable isotope approach. *Gondwana Res.* **2015**, *28*, 1500–1515. [CrossRef]
44. Greenwood, P.F.; Summons, R.E. GC-MS detection and significance of crocetane and pentamethylicosane in sediments and crude oils. *Org. Geochem.* **2003**, *34*, 1211–1222. [CrossRef]
45. Farzadnia, S.; Nimmagadda, R.D.; McRae, C. A comparative structural study of nitrogen-rich fulvic acids from various Antarctic lakes. *Environ. Chem.* **2018**, *14*, 502–514. [CrossRef]
46. Walters, C.C.; Moldowan, J.M. *The Biomarker Guide: Biomarkers and Isotopes In the Environment and Human History*; Cambridge University Press: Cambridge, UK, 2005.
47. Darnet, S.; Blary, A.; Chevalier, Q.; Schaller, H. Phytosterol Profiles, Genomes and Enzymes-An Overview. *Front. Plant Sci.* **2021**, *12*, 18. [CrossRef]
48. Tomazic, M.L.; Poklepovich, T.J.; Nudel, C.B.; Nusblat, A.D. Incomplete sterols and hopanoids pathways in ciliates: Gene loss and acquisition during evolution as a source of biosynthetic genes. *Mol. Phylogenetics Evol.* **2014**, *74*, 122–134. [CrossRef]
49. Fang, J.S.; Chan, O.; Joeckel, R.M.; Huang, Y.S.; Wang, Y.; Bazylinski, D.A.; Moorman, T.B.; Clement, B.J.A. Biomarker analysis of microbial diversity in sediments of a saline groundwater seep of Salt Basin, Nebraska. *Org. Geochem.* **2006**, *37*, 912–931. [CrossRef]
50. Hakimi, M.H.; Abdullah, W.H. Geochemical characteristics of some crude oils from Alif Field in the Marib-Shabowah Basin, and source-related types. *Mar. Pet. Geol.* **2013**, *45*, 304–314. [CrossRef]
51. Skret, U.; Fabianska, M.J. Geochemical characteristics of organic matter in the Lower Palaeozoic rocks of the Peribaltic Syneclise (Poland). *Geochem. J.* **2009**, *43*, 343–369. [CrossRef]
52. Peters, K.E.; Moldowan, J.M. *The Biomarker Guide: Interpreting Molecular Fossils in Petroleum and Ancient Sediments*; Prentice Hall: Hoboken, NJ, USA, 1993.
53. Irwin, H.; Meyer, T. Lacustrine organic facies—A biomarker study using multivariate statistical-analysis. *Org. Geochem.* **1990**, *16*, 197–210. [CrossRef]
54. Ma, S.H.; Zhang, S.C.; Su, J.; Wang, X.M.; He, K.; Fang, Y.; Mi, J.K. The Biomarkers in the Mesoproterozoic Organic-rich Rocks of North China Craton: Implication for the Precursor and Preservation of Organism in the Prokaryotic Realm. *Acta Geol. Sin.-Engl. Ed.* **2022**, *96*, 293–308. [CrossRef]
55. Fabianska, M.J.; Cmiel, S.R.; Misz-Kennan, M. Biomarkers and aromatic hydrocarbons in bituminous coals of Upper Silesian Coal Basin: Example from 405 coal seam of the Zaleskie Beds (Poland). *Int. J. Coal Geol.* **2013**, *107*, 96–111. [CrossRef]
56. Zhang, S.; Wu, T.; Zhang, S.; Cao, C.; Ma, W.; Shi, J.a.; Sun, G. Organofacies and paleoenvironment of lower Carboniferous mudstones (Dishuiquan Formation) in Eastern Junggar, NW China. *Int. J. Coal Geol.* **2015**, *150–151*, 7–18. [CrossRef]
57. Li, D.; He, D.; Santosh, M.; Ma, D.; Tang, J. Tectonic framework of the northern Junggar Basin part I: The eastern Luliang Uplift and its link with the East Junggar terrane. *Gondwana Res.* **2015**, *27*, 1089–1109. [CrossRef]
58. Li, D.; He, D.; Santosh, M.; Ma, D. Tectonic framework of the northern Junggar Basin Part II: The island arc basin system of the western Luliang Uplift and its link with the West Junggar terrane. *Gondwana Res.* **2015**, *27*, 1110–1130. [CrossRef]
59. He, D.; Chen, X.; Kuang, J.; Zhou, L.; Tang, Y.; Liu, D. Development and Genetic Mechanism of Chepaizi-Mosuowan Uplift in Junggar Basin, China. *Earth Sci. Front.* **2008**, *15*, 42–55. [CrossRef]
60. Pardo, J.D.; Small, B.J.; Milner, A.R.; Huttenlocker, A.K. Carboniferous–Permian climate change constrained early land vertebrate radiations. *Nat. Ecol. Evol.* **2019**, *3*, 200–206. [CrossRef] [PubMed]
61. Zhang, Y.X.; Wen, H.J.; Zhu, C.W.; Fan, H.F.; Cloquet, C. Cadmium isotopic evidence for the evolution of marine primary productivity and the biological extinction event during the Permian-Triassic crisis from the Meishan section, South China. *Chem. Geol.* **2018**, *481*, 110–118. [CrossRef]
62. Walliser, O.H. Global Events in the Devonian and Carboniferous. In *Global Events and Event Stratigraphy in the Phanerozoic: Results of the International Interdisciplinary Cooperation in the IGCP-Project 216 "Global Biological Events in Earth History"*; Walliser, O.H., Ed.; Springer: Berlin/Heidelberg, Germany, 1996; pp. 225–250.
63. Song, H.J.; Tong, J.N.; Xiong, Y.L.; Sun, D.Y.; Tian, L.; Song, H.Y. The large increase of delta C-13(carb)-depth gradient and the end-Permian mass extinction. *Sci. China-Earth Sci.* **2012**, *55*, 1101–1109. [CrossRef]
64. Bush, A.M.; Bambach, R.K. Paleoecologic Megatrends in Marine Metazoa. In *Annual Review of Earth and Planetary Sciences*; Jeanloz, R., Freeman, K.H., Eds.; Annual Review: San Mateo, CA, USA, 2011; Volume 39, pp. 241–269.
65. Kaiho, K.; Chen, Z.Q.; Ohashi, T.; Arinobu, T.; Sawada, K.; Cramer, B.S. A negative carbon isotope anomaly associated with the earliest Lopingian (Late Permian) mass extinction. *Palaeogeogr. Palaeoclimatol. Palaeoecol.* **2005**, *223*, 172–180. [CrossRef]
66. Kaiho, K.; Aftabuzzaman, M.; Jones, D.S.; Tian, L. Pulsed volcanic combustion events coincident with the end-Permian terrestrial disturbance and the following global crisis. *Geology* **2021**, *49*, 289–293. [CrossRef]
67. Lo, C.H.; Chung, S.L.; Lee, T.Y.; Wu, G.Y. Age of the Emeishan flood magmatism and relations to Permian-Triassic boundary events. *Earth Planet. Sci. Lett.* **2002**, *198*, 449–458. [CrossRef]
68. Abrajevitch, A.; Van der Voo, R.; Bazhenov, M.L.; Levashova, N.M.; McCausland, P.J.A. The role of the Kazakhstan orocline in the late Paleozoic amalgamation of Eurasia. *Tectonophysics* **2008**, *455*, 61–76. [CrossRef]
69. Xiao, W.; Santosh, M. The western Central Asian Orogenic Belt: A window to accretionary orogenesis and continental growth. *Gondwana Res.* **2014**, *25*, 1429–1444. [CrossRef]